Super-paramagnetic iron oxide nanoparticles for use in extrapulmonary tuberculosis diagnosis

C.-N. Lee[1], Y.-M. Wang[2], W.-F. Lai[3,8,9], T.-J. Chen[2], M.-C. Yu[4], C.-L. Fang[5], F.-L. Yu[4], Y.-H. Tsai[6], W. H.-S. Chang[7], C. S. Zuo[9] and P. F. Renshaw[9]

1) *Department of Pulmonary and Critical Care Medicine, Taipei Medical University-Shuang Ho Hospital, Taipei,* 2) *Department of Biological Science and Technology, National Chiao Tung University, Hsinchu,* 3) *Graduate Institute of Clinical Medicine, Taipei Medical University, Taipei,* 4) *Department of Internal Medicine, Taipei Medical University- Wanfang Hospital, Taipei,* 5) *Department of Pathology, Taipei Medical University, Taipei,* 6) *Department of Physical Medicine and Rehabilitation, Taipei Medical University Hospital, Taipei,* 7) *Department of Biomedical Engineering, Chung Yuan Christian University, Chung Li,* 8) *Center for Nano-Tissue Engineering and Image Research, Taipei Medical University Hospital, Taipei, Taiwan and* 9) *Brain Imaging Center, McLean Hospital/Harvard Medical School, Belmont, MA, USA*

Abstract

The limited sensitivity of serological tests for mycobacterial antigens has encouraged the development of a nanoparticle probe specific for the extrapulmonary form of *Mycobacterium tuberculosis* (Mtb). We developed an innovative probe comprised of super-paramagnetic iron oxide (SPIO) nanoparticles conjugated with Mtb surface antibody (MtbsAb-nanoparticles) to provide ultrasensitive imaging of biomarkers involved in extrapulmonary Mtb infection. MtbsAb-nanoparticles were significantly conjugated with Mtb bacilli. The extent of contrast enhancement reduction on magnetic resonance imaging (MRI) for Mtb and human monocytic THP1 cells was proportional to the concentration of MtbsAb-nanoparticles. When MtbsAb-nanoparticles were intravenously injected into mice bearing Mtb granulomas, the granulomatous site showed a 14-fold greater reduction in signal intensity enhancement on T_2-weighted MR images compared with an opposing site that received PBS injection. Mtb sAb-nanoparticles represent a new non-invasive technology for the diagnosis of extrapulmonary Mtb.

Keywords: Diagnosis, extrapulmonary, magnetic resonance imaging, *Mycobaterium tuberculosis*, nanoparticle
Original Submission: 14 September 2011; **Revised Submission:** 26 December 2011; **Accepted:** 6 February 2012
Editor: M. Drancourt
Article published online: 24 February 2012
Clin Microbiol Infect 2012; **18:** E149–E157
10.1111/j.1469-0691.2012.03809.x

Corresponding author: W.-F. T. Lai, Graduate Institute of Medical Sciences, Taipei Medical University, 250 Wuhsing St., Taipei, Taiwan 110, China
E-mail: laitw@tmu.edu.tw
and
Brain Imaging Center, McLean Hospital/Harvard Medical School, Belmont, MA 02478, USA
E-mail: tlai@mclean.harvard.edu
Y. M. Wang, Department of Biological Science and Technology, National Chiao Tung University, Hsinchu 300, Taiwan

Introduction

Tuberculosis (TB) is a major public health problem that affects nearly one-third of the world's population [1]. For example, in 2005, 8.8 million new TB cases and 1.6 million deaths attributed to TB were reported, making TB the second leading cause of infectious disease deaths [2]. Extrapulmonary TB (ETB) is an even greater diagnostic challenge than primary TB (PTB), as it occurs less frequently and with little liberation of bacilli. In addition, it is usually localized at sites that are difficult to access, such as lymph nodes, the pleura and osteoarticular areas [3] Further, invasive procedures required to obtain adequate clinical specimens are complex and sometimes risky, which makes bacteriological confirmation difficult, thus requiring more invasive procedures to obtain adequate samples [4–6]. Also in ETB, fewer bacilli cause much greater damage secondary to bacterial invasion of solid organs, which induces severe immunological reactions. Thus, the combination of small numbers of bacilli

and inaccessible sites makes bacteriological confirmation of extrapulmonary TB more difficult [7].

The diagnosis of extrapulmonary mycobacterial infection is also difficult to establish due to its non-specific clinical presentation. Negative sputum smears for acid-fast bacilli, lack of granulomatous tissue on histopathology or failure to culture *Mycobacterium tuberculosis* do not exclude a diagnosis.

Currently, commercial antibody detection tests for ETB serve no role in clinical care or case detection due to their highly variable sensitivities (range, 0.00–1.00) and specificities (range, 0.59–1.00) for all extrapulmonary sites combined [8]. Enzyme-linked immunospot (ELISPOT) assay for interferon-γ, a cytokine produced by activated T cells after exposure to *Mycobacterium tuberculosis* (Mtb) antigens, early secretory antigenic target 6 (ESAT-6) and culture filtrate protein 10 (CFP-10) have been used for the diagnoses of latent and active TB; however, results vary between different disease sites and few studies have investigated the specificities and sensitivities of these assays for diagnosing extrapulmonary TB [9–11]. Thus, novel diagnostic modalities are needed.

Additional tests for ETB are frequently negative, including negative skin PPD tests and pseudo-negative QuantiFERON-TB tests [12]. Although QuantiFERON TB-2G and immune-based blood assays, which do not require a specimen from the affected organ for microbiological or histological examination, may serve as alternative diagnostic tools [9,13,14]. Other TB diagnostic methods include serological tests by enzyme-linked immunosorbent assays (ELISA), which do not have sufficient sensitivity and specificity to be useful [15,16].

The development of DNA amplification techniques, such as the polymerase chain reaction (PCR), shows promise. However, their use in TB diagnosis is limited as most studies to date only used small sample sizes with poorly explained reference standards and clinical criteria, making comparisons among these studies difficult [17,18]. Other disadvantages of using PCR are the need for an adequate infrastructure and personnel qualified to perform this technique [7]. Therefore, an ideal test for latent ETB is still urgently needed.

Advances in molecular imaging are aimed at developing and testing novel methods that can image specific molecular pathways *in vivo*, particularly those directly involved in disease processes [19,20]. The detection of biological materials using organic fluorescent labelling has become widespread in the life sciences, including biological imaging and diagnostics [21]. Functional limitations of organic fluorescent dyes used in biotechnology applications have resulted in the development of new labelling systems [22]. Highly sensitive and highly specific probes that lack the intrinsic limitations of organic dyes and fluorescent proteins are of considerable interest in many research areas [22,23].

Luminescent colloidal nanometer-sized semiconductor particles have the potential to overcome the intrinsic limitations of organic fluorescent dyes [24–26]. These nanocrystals have been covalently linked to biorecognition molecules, such as peptides, antibodies, nucleic acids and small-molecule ligands, for use as fluorescent probes [27–29]. Compared with organic fluorophores, these quantum dots (QDs) have unique optical and electronic properties, including size- and composition-tunable fluorescence emissions ranging from visible to infrared wavelengths, large absorption coefficients across a wide spectral range and high brightness levels and photostability. So long as the semiconductor core is well encapsulated, the specific photochemical reactions that cause organic dyes to photobleach are not a problem with inorganic nanoparticles. Due to their broad excitation profiles and narrow, symmetric emission spectra, they are also well suited for optical multiplexing to encode genes, proteins and small-molecule libraries.

Recently, super-paramagnetic iron oxide (SPIO) nanoparticles have been used to increase the sensitivity and specificity of MRI systems [30,31]. These clearly delineate precise structures at the molecular level and provide a valuable tool to thoroughly study antibody–antigen and parasite–host interactions.

We have designed a new molecular imaging probe comprised of SPIO nanoparticles conjugated with Mtb surface antibody (MtbsAb-nanoparticles). SPIO nanoparticle probes have the advantage of being non-toxic, or minimally toxic to cells and tissues under normal physiological conditions [32,33]. In addition, due to their paramagnetic properties, they can be detected at low concentrations and provide precise magnetic resonance images at the molecular level. Moreover, iron oxide paramagnetic nanoparticles incur no risk of allergic immune reactions, as iron ions participate in normal physiological metabolism.

In this exploratory study, we evaluated the sensitivity and specificity of these probes using both *in vitro* cell cultures and *in vivo* animal assays with the goal of developing an ultrasensitive imaging agent for detecting extrapulmonary mycobacterial infection.

Methods

All reagents used for synthesis were purchased from commercial sources. These included: ferric chloride hexahydrate ($FeCl_3{\cdot}6H_2O$), ferrous chloride tetrahydrate ($FeCl_2{\cdot}4H_2O$) and NH_4OH from Fluka, Seelze, Germany; epichlorohydrin, 2,2′-(ethylenedioxy)bis(ethylamine) (EDBE), 1-hydroxybenzotriazole (HOBt) and (benzotriazol-1-yloxy) tripyrrolidinophosphonium hexafluorophosphate (PyBop) from Sigma-Aldrich,

Seelze, Germany; dextran (T-40), Sephacryl S-300 and Sephadex G-25 from GE Healthcare Bio-sciences AB, Uppsala, Sweden; and SPECTRUM molecular porous membrane tubing from Spectrum Laboratories Inc, Rancho Dominguez, CA, USA. TB surface antibodies (TB surface antibody- Polyclonal Antibody to Mtb (Rabbit anti-M tuberculosis) BP2027) were purchased from Acris Antibodies GmbH, Im Himmelreich, Hiddenhausen.

Synthesis of SPIO

Magnetic iron oxide coated dextran nanoparticles were prepared by mixing dextran T-40 (5 mL; 50% w/w) with an aqueous solution containing $FeCl_3{\cdot}6H_2O$ (0.45 g; 2.77 mmol) and $FeCl_2{\cdot}4H_2O$ (0.32 g; 2.52 mmol). The mixture was stirred vigorously at room temperature followed by the rapid addition of NH_4OH (10 mL; 7.5% v/v). The resulting black suspension was stirred continuously for 1 h and subsequently centrifuged at 17 300 *g* for 10 min in order to remove aggregated material. The super-paramagnetic iron oxide nanoparticles (SPIO) were separated from unbound dextran T-40 by gel filtration chromatography with Sephacryl S-300. The reaction mixture (5 mL) was applied to a 2.5 × 33 cm column and eluted with buffer solution containing 0.1 M Na acetate and 0.15 M NaCl at pH 7.0. The purified magnetic iron oxide coated dextran nanoparticles were collected in the void volume, and column eluates were assayed for iron at 330 nm by hydrochloric acid and for dextran at 490 nm by the phenol/sulphuric acid method [34].

The iron oxide coated dextran nanoparticles were proven by FT-IR. FT-IR (KBr)(cm^{-1}): $\tilde{\nu}$ = 3300 (O–H), 2800 (–CH_2– stretch).

Synthesis of SPIO-EDBE-SA

We synthesized SPIO conjugated with EDBE using previously reported methods [35,36]. SPIO-EDBE and succinic anhydride (1 g, 10 μmol; SA) in NaOH (5 M; 10 mL) was stirred for 24 h at room temperature; the solution was dialyzed using SPECTRUM molecular porous membrane tubing (12 000–14 000 MW cut-off) against 20 changes of distilled water (2 L each).

Synthesis of SPIO-MtbsAb

SPIO-EDBE-SA (100 μL) at a concentration of 4 mg/mL of Fe was added to 400 μL (4.5 mg/mL) *M. tuberculosis* (BP2027; Acris, Himmelreich, Germany) Ab using 1-hydroxybenzotriazole (HOBt) and (benzotriazol-1-yloxy) tripyrrolidinophosphonium hexafluorophosphate (PyBop) as catalysts, then stirred for 24 h at room temperature. The solution was separated from unbound antibody by gel filtration chromatography on Sephadex G-25. The reaction mixture (5 mL) was applied to a 2.5 × 33 cm column and eluted with PBS buffer. The formation of Ab–nanoparticles was confirmed with a bicinchoninic acid protein assay kit [37].

Transmission electron microscope (TEM) measurements

Particle average core size, size distribution and morphology were evaluated using a transmission electron microscope (JEOL JEM-2000 EX II; Tokyo, Japan) at a voltage of 100 kV. The composite dispersion was drop-cast onto a 200-mesh copper grid (Agar Scientific, Emitek, Ashford, UK), which was then air-dried at room temperature before loading onto the microscope.

Relaxation time measurements

Relaxation time values (T_1 and T_2) of the aqueous solution of MtbsAb-nanoparticles were measured to determine relaxivities: r_1 and r_2. All measurements were made using a NMR relaxometer (NMS-120 Minispec, Bruker, Bremen, Germany) operating at 20 MHz and 37.0 ± 0.1°C. Before each measurement, the relaxometer was tuned and calibrated. Both r_1 and r_2 values were determined from eight data points generated by inversion-recovery and a Carr-Purcell-Meiboom-Gill pulse sequence.

Mycobacteria

The vaccination strain used was *M. bovis* BCG Pasteur Mérieux, which was grown to mid-log phase in Middlebrook 7H9 broth (Difco, Sparks, MD, USA) supplemented with 10% (v/v) ADC, 0.05% (v/v) Tween 80 and 0.2% (v/v) glycerol at 37°C. Cultures were aliquoted into 1 mL tubes and stored at −80°C until use. Thawed aliquots were diluted with double-distilled sterile water to the desired inoculum concentrations. The use of *M. bovis* BCG in this study was limited by biosafety and grading of the author's laboratory. The lyophilized vaccine/bacteria stock was reconstituted with Sauton's medium and then diluted with ddH_2O for further use.

Acid-fast bacteria Ziehl–Neelsen stain and Berlin blue stain

Tuberculosis smears to examine for positive acid-fast bacilli used Ziehl–Neelsen staining, as previously described [38]. SPIO MtbsAb probes were incubated with Mtb broth for 30 min and then stained with Berlin blue to determine if the probe conjugated to the bacteria [39].

***In vitro* cell culture and imaging**

Human monocytic THP-1 cells were cultured in RPMI 1640 (Gibco/Invitrogen, Carlsbad, CA, USA) supplemented with 10% fetal bovine serum (FBS) (Gibco/Invitrogen), 50 mg/L gentamycin sulfate (Gibco), 100 units/mL penicillin G sodium (Gibco), 100 μg streptomycin sulphate (Gibco) and 0.25 mg/L fungizone (Gibco). We used THP-1 cells because monocytes

represent the first site of bacterial contact in extrapulmonary infection. Cells were cultured in a 5% CO_2 incubator at 37°C.

Super-paramagnetic iron oxide TBsAb probes (2 mM) were incubated with 10^6 CFU *M. bovis* BCG only or with 10^6 CFU *M. bovis* BCG pre-incubated with 1×10^7 activated THP-1 cells in 1 mL Eppendorf tubes in a 5% CO_2 incubator at 37°C for 1 h. The tubes were then centrifuged and the supernatant was removed. The pellets were redissolved in 200 μL of medium. MRI scans (3.0-T, Sigma; GE Medical Systems, Milwaukee, WI, USA) were performed to evaluate the sensitivity and specificity of the probes using the *in vitro* cell culture system. All samples were scanned with a fast gradient echo pulse sequence (TR/TE/flip angel 500/20/10°).

Mice

Five C57BL/6 mice were obtained from the animal facilities at Taipei Medical University. The mice were housed individually in polycarbonate cages in a temperature- and humidity-controlled environment. Ambient lighting was automatically controlled to provide 12-h light and 12-h dark cycles. The mice were kept under specific pathogen-free conditions and fed autoclaved food and water *ad libitum*. All procedures were reviewed and approved by the Taipei Medical University Laboratory Animal Care Committee. At 8 weeks of age, the mice were housed in appropriate biological containment facilities at Wang-Fan Hospital under barrier conditions in a biosafety level III animal laboratory. Following local ethical review, all animal work was carried out in accordance with the Animal (Scientific Procedures) Act of 1986.

BCG vaccination

Mice were inoculated with a live attenuated strain of *M. bovis* BCG (Connaught strain; ImmuCyst Aventis) that was provided by Pasteur Mérieux. On the day of inoculation, the lyophilized vaccine/ bacteria stock was first reconstituted in Sauton's medium and then diluted with saline to the desired concentration. A volume of 0.1 mL per mouse was then injected intradermally into the left or right dorsal scapular skin. A dose of 10^7 CFU per mouse was selected based on methods described in the literature [40]. Negative control mice were given saline. After 1 month, infection was verified by histology of bacteria-inoculated tissue samples.

Histology and immunohistochemistry

Bacteria inoculated-tissue samples were removed *en bloc* and fixed in 10% formalin. The tissues were then embedded in paraffin and serially sectioned (Sacura Sledge microtome) at 5–10 μm. Tissue sections were stained with Hematoxylin/ Eosin, Ziehl–Neelsen for acid-fast bacteria [38] and Berlin blue for ferric iron [39].

Immunohistochemistry used a modification of the avidin-biotin-peroxidase complex (ABC) technique. Deparaffinized sections were incubated with rabbit (primary) Ab against *M. tuberculosis* (1:100 dilution, BP2027; Acris, Himmelreich, Germany) for 4 h, and with a secondary biotinylated goat Ab against rabbit-IgG (1:200 dilution, 21538; IHC Select, Millipore, Billerica, MA, USA) at room temperature. Complexes were disclosed with a chromogen of oxidized diaminobenzidine-H_2O_2 reaction. Slides were viewed using a Nikon Eclipse 800 microscope (Nikon Corporation, Tokyo, Japan) and images were digitally captured using a CCD-SPOT RT digital camera (Diagnostic Instruments Inc., Sterling Heights, MI, USA) and then compiled using Adobe Photoshop™ CS3 software (Adobe Systems Inc., San Jose, CA, USA). Bacterial clumps and acid-fast bacilli were observed at ×3000 total magnification under oil.

In vivo MR imaging

MRI was performed on all mice before and, once every 5 min, for a total of 30 min, after probe injection. Five mice were anaesthetized for imaging via subcutaneous injection of Ketamine (80 mg/kg of body weight) and Xylazine (12 mg/kg). SPIO-TBsAb probes (2 nmol/200 μL) were injected intravenously through a tail vein. For MR imaging, T_2-weighted fast spin-echo imaging was used (TR = 3000; TE = 90; field of view = 8). The same radiologist did the quantitative analyses for all MR images. Signal intensity (SI) was measured in defined regions of interest (ROI), which were in comparable locations within a TB granulomatous lesion centre. In addition, the SI in the ROI of the back muscle adjacent to the granulomatous area was measured. The ROI size was chosen as 2/3 of the maximum diameter of the granulomatous area. Relative signal enhancement was calculated using the SI measurements prior to (SIpre) and after (SIpost) injection of the contrast agents using the formula $[(SIpost-SIpre)/SIpre] \times 100$, where SIpre was the lesion signal intensity on the pre-enhanced scan (control) and SIpost was the lesion signal intensity on the post-enhanced scan at 0–3 h.

Statistical analysis

Results are given as means + SDs. Statistical comparisons used two-tailed Student's *t*-tests. A p-value <0.05 was considered to be significant.

Results

Synthesis and characterization of SPIO-TBsAb

The surface of an SPIO particle was modified to enable conjugation with TBsAb. Initially, dextran immobilized on the

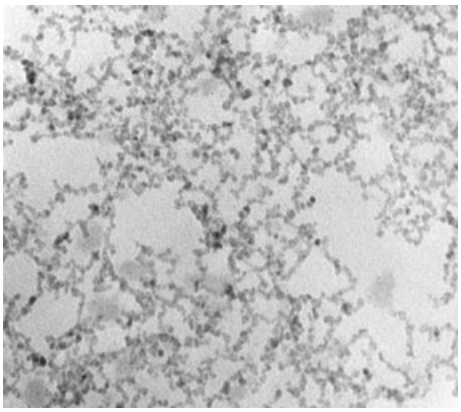

FIG. 1. TEM image of MtbsAb-nanoparticles. The average core size of MtbsAb-nanoparticles is 3.8 ± 0.4 nm. (Bar = 15 nm).

SPIO nanoparticles was cross-linked by epichlorohydrin. Subsequently, the SPIO nanoparticles were treated with EDBE to generate primary amine functional groups at the dextran ends. Then, succinic anhydride (SA) was added to form SPIO-EDBE-SA. Finally, TBsAb was conjugated with SPIO–EDBE-SA in the presence of coupling agents to form SPIO-TBsAb.

Figure 1 shows a TEM image of TBsAb-nanoparticles. This TEM image indicates that the TBsAb-conjugated iron oxide nanoparticles were well dispersed. The mean core size of the TBsAb-nanoparticles was 3.8 ± 0.4 nm (calculated using 200 particles).

In aqueous solution, the relaxivity values, r_1 and r_2, of the TBsAb-nanoparticles at 37.0 ± 0.1°C and 20 MHz were 23 ± 3 and 151 ± 8 mM/s, respectively. These were slightly lower than those of Resovist (r_1 = 26 and r_2 = 164 mM/s). However, the (r_1/r_2) ratio of TBsAb-nanoparticles was similar to that of Resovist.

In vitro characterization and imaging

To characterize the SPIO TBsAb probe, we first examined *M. bovis* BCG using Ziehl–Neelsen staining for acid-fast bacteria (Fig. 2a). The probes were then conjugated with bacteria and identified by ferric iron staining with Berlin blue (Fig. 2b).

The SPIO TBsAb probes that targeted Mtb were confirmed by T_2-weighted MR imaging; reduced enhancement was shown for probes incubated with bacteria. The reduction of signal intensity (SI) in the presence of SPIO probes was concentration dependent (Fig. 2c). SPIO probes of 2, 1 and 0.5 mM conjugated with TB showed SIs, respectively, of 97.67 + 3.05, 131.67 + 4.51 and 257.33 + 5.03, which were comparable to the probe alone (1 mM: SI = 90.75 + 2.47). Almost no signal reduction (SI = 957.33 + 12.53) was found for the TB only group compared with PBS (SI = 1073.43 + 13.62). This

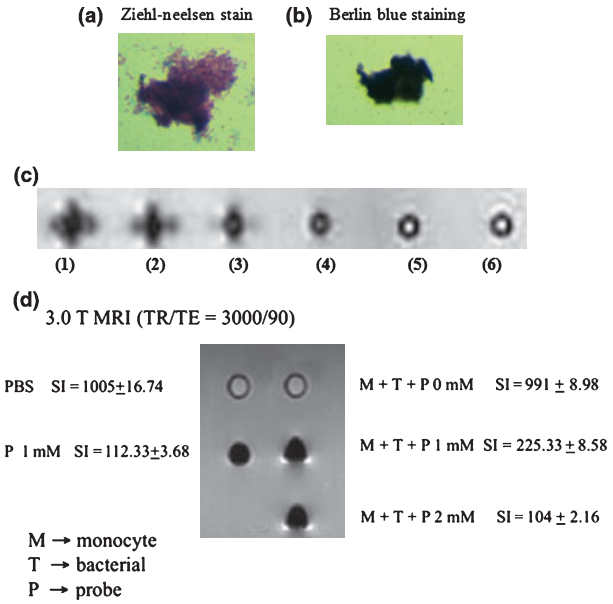

FIG. 2. *In vitro* and cell characterization of SPIO MtbsAb. (a) Ziehl–Neelsen staining to identify acid-fast bacilli and (b) Berlin blue staining to identify the ferric iron of SPIO probes conjugated to bacteria. Negative contrast enhancement of T_2-weighted MR images is shown for the SPIO MtbsAb probes incubated with bacteria. The signal intensity (SI) is reduced by the presence of SPIO probes in a dose-dependent manner: (1) 90.75 + 2.47 (1.0 mM Probe); (2) 97.67 + 3.05 (Mtb + 2.0 mM Probe); (3) 131.67 + 4.51 (Mtb + 1.0 mM Probe); (4) 257.33 + 5.03 (TB + 0.5 mM Probe); (5) 957.33 + 12.53 (Mtb + 0 mM Probe); (6) 1073.43 + 13.62 (PBS). (c) No signal reduction is found in the PBS control group. (d) Similar dose-dependent negative enhancement is also found 1 h after bacteria-conjugated SPIO probes are incubated with THP-1 monocytes.

indicated that the SPIO probes specifically targeted TB bacilli, and the decline in SI on the enhanced MRI images for SPIO probes was also consistent with iron oxide particles.

A similar decrease in SI on enhanced MR images was found 1 h after the bacteria-conjugated SPIO probes were incubated with THP-1 monocytes. SI was significantly reduced in the TB group with the 1 mM probes (SI = 225.33 + 8.58) and 2 mM probes (SI = 104 + 2.16) compared with the control group without the probe (SI = 991 + 8.98) and the PBS only group (SI = 1005.33 + 16.74). Similar reductions in MRI enhancements in the TB groups with 1 and 2 mM probes were comparable to the positive 1.0 mM probe only group (SI = 112.33 + 3.68). Thus, the SPIO TBsAb probe was applicable to TB probe-activated THP-1 monocyte trafficking.

In vivo imaging

To check if TB infection could be detected by MR imaging *in vivo*, SPIO TBsAb probes were intravenously administered to

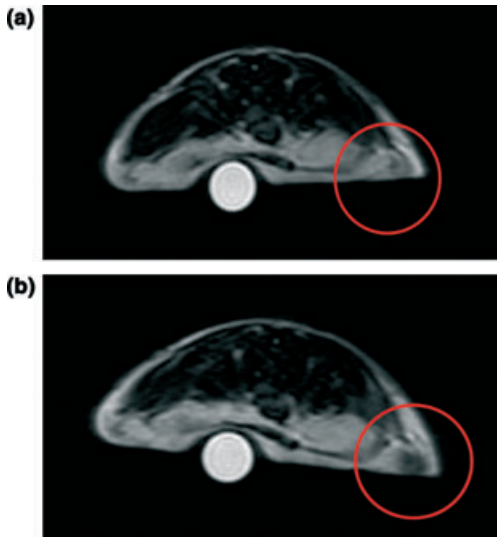

FIG. 3. *In vivo* SPIO TBsAb imaging in subcutaneous TB lesions of a C57BL/6 mouse. A significant 14-fold reduction in MR signal intensity was found in the TB granulamatous areas compared with the control areas 1 h after probe injection (−23.43 + 7.24 and −1.68 ± 1.32, p <0.001). (a) Pre-injection and (b) post-injection.

TB-infected mice. At ½ h later, a clearly detectable MR signal was observed in the TB granulomatous area, although the highest target to background signal was observed at the 1-h time point. As shown in Fig. 3, a significant reduction of MR signalling was found in TB granulomatous areas.

Signal enhancement evaluations used SI measurements prior to (SIpre) and after (SIpost) injection of the contrast agent. The T_2-weighted reduction in signal enhancement was *c.* 14-fold greater at the TB granulamatous sites compared with the control sites 1 h after probe injection (−23.43 + 7.24% and −1.68 ± 1.32%; p <0.001).

Histology and immunohistochemistry

In C57BL/6 mice, the subcutis developed a granulomatous lesion 1 month after infection. Some blood vessels could be seen within these lesions along with aggregates of lymphocytes and epithelioid macrophages. The development of these organized granulomas was progressive (Fig. 4a). To examine if the TB lesions were correlated with the SPIO-MtbsAb MR signals, immunohistochemistry was performed using anti-MtbsAb, which indicated the interaction of TB Ag with TB Ab.

Immunohistochemical staining for MtbsAb expression was noted in the granulomatous areas (Fig. 4b). Acid-fast bacilli were scattered within the same lesion (Fig. 4c). Berlin blue was then used to stain for ferric iron, which indicated the probes' conjugation to TB bacteria. Berlin blue staining SPIO probes were located in the same area as MtbsAb (Fig. 4d). Figure 4a–d shows co-localized pairs.

Discussion

The limited sensitivities of serological tests for detecting mycobacterial antigens have encouraged the development of more specific tests to diagnose the extrapulmonary form of TB (ETB). An innovative probe comprised of super-paramagnetic iron oxide (SPIO) nanoparticles conjugated with Mtb surface antibody (MtbsAb-nanoparticles) was used to target Mycobacterial antigens, which provided ultrasensitive imaging of biomarkers involved with ETB infection. Previous investigations to detect TB bacteria in relatively large sputum sample volumes used hybrid nanoparticles with a large iron core and a thin ferrite shell (cannonballs (CB)) [41]. Our results showed that MtbsAb-nanoparticles were significantly conjugated with TB bacilli, in agreement with previous studies [41]. Notably, the extent of contrast enhancement reduction on magnetic resonance imaging for TB and monocytic THP1 cells was proportional to the concentration of MtbsAb-nanoparticles.

One major problem with ETB is its low activity in the body, which makes its detection difficult. When TBsAb-nanoparticles were administered to mice bearing TB granulomas by intravenous injection, the granulomatous site was detected on T_2-weighted magnetic resonance images as a 14-fold greater reduction in signal enhancement compared with an opposing site with PBS injection, indicating a significant accumulation of contrast agent. This suggests the possibility of obtaining specific targeting with a contrast agent, which could result in lower required doses for clinical diagnosis.

Our results indicate that SPIO nanoparticles accumulate in detectable amounts in TB granulomatous lesions. These findings further support the development of an SPIO probe using an anti-human TB Ab. Because the magnetic iron oxide core

FIG. 4. Correlations of HE, TB Ab, acid-fast and Berlin blue staining. The subcutaneous granulomatous lesions predominantly include lymphocytes and epithelioid macrophages. New blood vessel formation and large aggregates of lymphocytes and epithelioid macrophages are found in these lesions. (a) The development of organized granulomas appears to be progressive. (b) Immunohistochemical staining for MtbsAb expression is noted in the granulomatous area, whereas (c) acid-fast bacilli are scattered within the same lesions. (d) Berlin blue staining SPIO probes are noted in the same area as MtbsAb. Berlin blue stains for ferric iron, which indicates the probes' conjugation with TB bacteria.

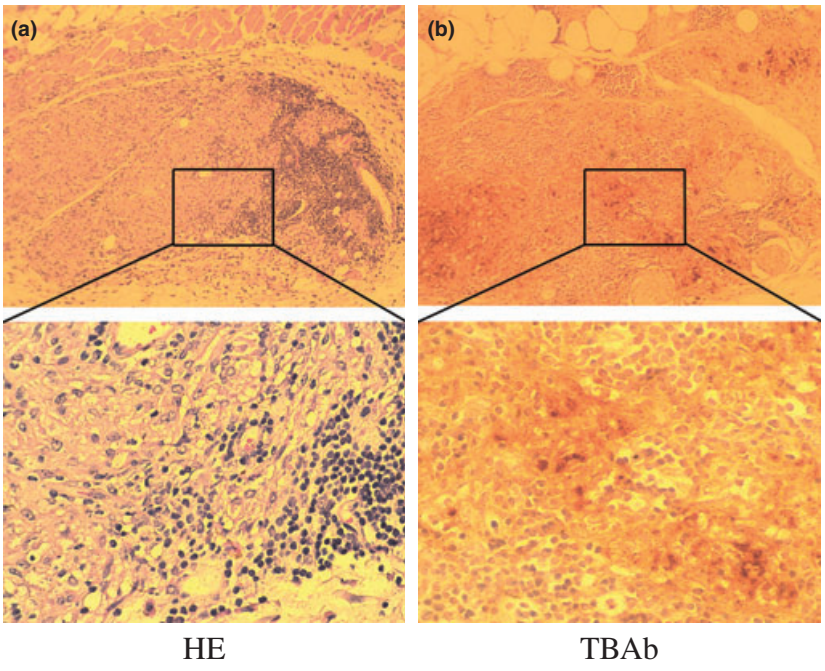

HE TBAb

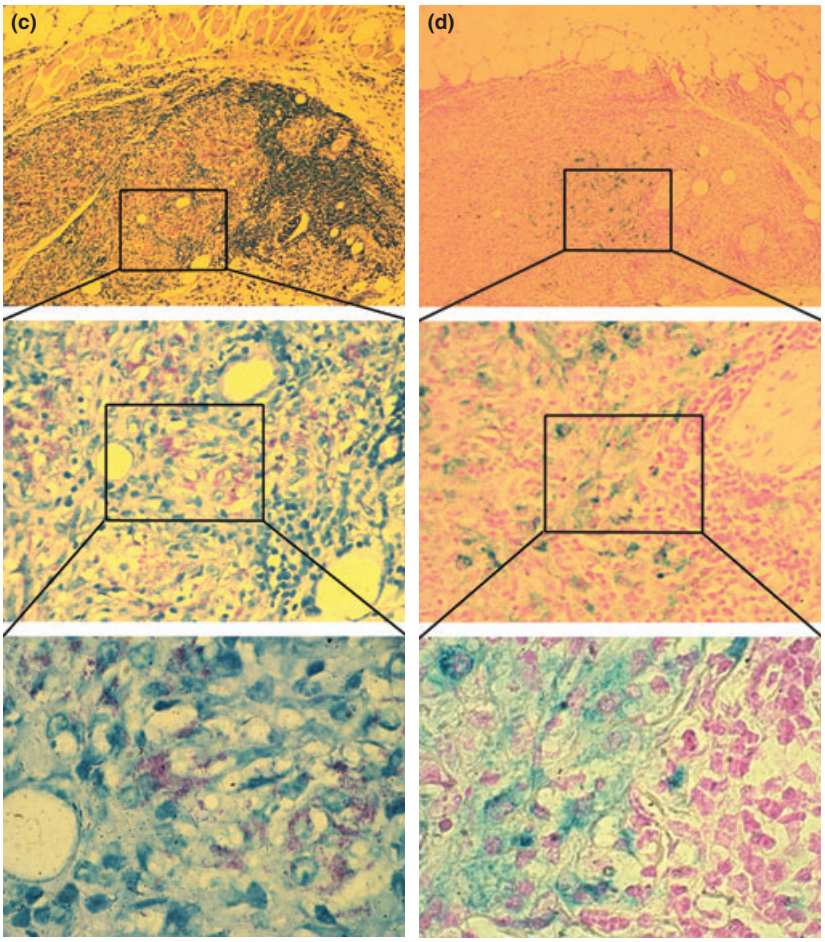

of SPIO-HD is widely used in MRI contrast agents to induce T_2 shortening, our results indicate the potential to image similar cell behaviours in patients in a non-invasive manner. This would allow the evaluation of existing treatment protocols or modified protocols, which might ultimately provide more favourable patient outcomes. Thus, MtbsAb-nanoparticles may constitute a new non-invasive technology for the diagnosis of extrapulmonary tuberculosis.

For this exploratory study, we used *M. bovis* BCG and rabbit anti-M tuberculosis as the antigen and antibody, respectively. The cross-reactivity between rabbit and bovine sources was not considered to be too high, although our results demonstrated that SPIO conjugated with specific TB antibodies showed significant interactions with bovine BCG bacteria. A dose-dependent reduction in signal enhancement was shown for probes incubated with bacteria. This indicates that SPIO probes specifically target TB, and the enhancement decline seen on MRI for SPIO probes was also consistent with the presence of iron oxide particles. However, additional studies are warranted to investigate other, more specific antibodies or antibody combinations to improve specificity.

The subcutis developed a TB granulamatous lesion 1 month after infection in this mouse model. Typical TB granulomatous histology findings were identified, including the presence of lymphocytes, epithelioid macrophages and new blood vessel formation. Acid-fast bacilli were scattered in the TB lesions, which corroborated the MtbsAb immunohistochemistry findings. This indicated an interaction between Mtb Ag and Mtb Ab. The ferric iron stain Berlin blue highlighted the same areas with MtbsAb, which indicated the probes' conjugation with TB bacteria.

Previous reports have shown that SPIO probes are not cytotoxic and do not influence cell behaviour at particle concentrations comparable to those we have used [32, 33, 42–44]. Our results showed minimal influence 1 h after the bacteria-conjugated SPIO probe was incubated with THP-1 monocytes. SI was significantly reduced in the groups with TB and with 1 mM probes (SI = 225.33 + 8.58) and 2 mM probes (SI = 104 + 2.16) compared with those groups without the probe (SI = 991 + 8.98) and PBS only (SI = 1005.33 + 16.74). Although the SPIO MtbsAb probe is a promising tool for Mtb probe-activated THP-1 monocyte trafficking, additional investigations will be necessary using different bacterial loads in order to evaluate probe sensitivity.

Our study had several limitations. We did not observe the biodistribution of the SPIO MtbsAb probe in this study. Another important limitation involved limited data for the intravascular half-life of the SPIO Ab probe and its possible liver deposition, which could affect the time that the particles are exposed to THP-1 monocytes located within a TB lesion. This remains a subject for further investigation. In addition, MRI cannot determine if SPIO nanoparticles are specifically bound to bacteria/monocytes or if these particles are endocytosed. This also remains a subject for future research.

In conclusion, we have successfully prepared and characterized biocompatible SPIO-MtbsAb nanoparticles. These nanoparticles are hydrophilic, minimally cell cytotoxic at low concentrations, and well dispersed under physiological conditions. Moreover, MtbsAb-nanoparticles can target and detect TB infection, as shown by both *in vitro* and *in vivo* MRI studies. Therefore, SPIO-MtbsAb nanoparticles may be used as MRI contrast agents for detecting extrapulmonary TB.

Acknowledgements

This study was funded by the National Science Council of Taiwan (grants NSC 94-2320-B-038-013, NSC 99-2120-B-038-001).

Transparency Declaration

No conflict of interest to be declared.

References

1. Lauzardo M, Ashkin D. Phthisiology at the dawn of the new century: a review of tuberculosis and the prospects for its elimination. *Chest* 2000; 17: 1455–1473.
2. World Health Organization. *Global tuberculosis control, surveillance, planning, financing*. Geneva, Switzerland: World Health Organization. WHO Report. 2007.
3. Small PM, Schecter GF, Goodman PC, Sande MA, Chaisson RE, Hopewell PC. Treatment of tuberculosis in patients with advanced human immunodeficiency virus infection. *N Engl J Med* 1991; 324: 289–294.
4. Alvarez S, McCabe WR. Extrapulmonary tuberculosis revisited: a review of experience at Boston City and other hospitals. *Medicine (Baltimore)* 1984; 63: 25–55.
5. Ozbay B, Uzun K. Extrapulmonary tuberculosis in high prevalence of tuberculosis and low prevalence of HIV. *Clin Chest Med* 2002; 23: 351–354.
6. Ebdrup L, Storgaard M, Jensen-Fangel S, Obel N. Ten years of extrapulmonary tuberculosis in a Danish university clinic. *Scand J Infect Dis* 2003; 35: 244–246.
7. García-Elorriaga G, Gracida-Osorno C, Carrillo-Montes G, Gonzalez-Bonilla C. Clinical usefulness of the nested polymerase chain reaction in the diagnosis of extrapulmonary tuberculosis. *Salud Pública de México* 2009; 51: 240–245.
8. Steingart KR, Henry M, Laal S *et al.* A systematic review of commercial serological antibody detection tests for the diagnosis of extrapulmonary tuberculosis. *Postgrad Med J* 2007; 83: 705–712.
9. Liao CH, Chou CH, Lai CC *et al.* Diagnostic performance of an enzyme-linked immunospot assay for interferon-g in extrapulmonary

tuberculosis varies between different sites of disease. *J Infect* 2009; 59: 402–408.
10. Kim SH, Choi SJ, Kim HB, Kim NJ, Oh MD, Choe KW. Diagnostic usefulness of a T-cell-based assay for extrapulmonary tuberculosis. *Arch Intern Med* 2007; 167: 2255–2259.
11. Kim SH, Song KH, Choi SJ *et al.* Diagnostic usefulness of a T-cell-based assay for extrapulmonary tuberculosis in immunocompromised patients. *Am J Med* 2009; 122: 189–195.
12. Pai M, Zwerling A, Menzies D. Systematic review: T-cell-based assays for the diagnosis of latent tuberculosis infection: an update. *Ann Intern Med* 2008; 149: 177–184.
13. Koashi Y, Mouri K, Yagi S, Obase Y, Miyashita N, Oka M. Clinical utility of a T cell-based assay in the diagnosis of extrapulmonary tuberculosis. *Respirology* 2009; 14: 276–281.
14. Paluch-Oleś J, Magrys A, Kot E, Koziol-Montewka M. Rapid identification of tuberculosis epididymo-orchitis by INNO-LiPA Rif TB and QuantiFERON-TB Gold In Tube tests: case report. *Diagn Microbiol Infect Dis* 2010; 66: 314–317.
15. Kaneko K, Onodera O, Miyatake T, Tsuji S. Rapid diagnosis of tuberculous meningitis by polymerase chain reaction (PCR). *Neurology* 1990; 40: 1617–1618.
16. Bhigjee AI, Padayachee R, Paruk H, Hallwirth-Pillay KD, Marais S, Connoly C. Diagnosis of tuberculous meningitis: clinical and laboratory parameters. *Int J Infect Dis* 2007; 11: 348–354.
17. Barnes P. Rapid diagnostic test of tuberculosis: progress but no gold standard. *Am J Respir Crit Care Med* 1997; 155: 1497–1498.
18. Kumar P, Nath K, Rath B *et al.* Visual format for detection of *Mycobacterium tuberculosis* and *M. bovis* in clinical samples using molecular beacons. *J Mol Diagn* 2009; 11: 430–438.
19. Miyawaki A, Sawano A, Kogure T. Lighting up cells: labelling proteins with fluorophores. *Nat Cell Biol* 2003; September (suppl): S1–S7.
20. Weissleder R, Mahmood U. Molecular imaging. *Radiology* 1996; 219: 316–333.
21. Schrock E, du Manoir S, Veldman T. Multicolor spectral karyotyping of human chromosomes. *Science* 1996; 273: 494–497.
22. Jaiswal JK, Simon SM. Potentials and pitfalls of fluorescent quantum dots for biological imaging. *Trends Cell Biol* 2004; 14: 497–504.
23. Lai WF, Chang CH, Tang Y, Bronson R, Tung CH. Early diagnosis of osteoarthritis using cathepsin B sensitive near-infrared fluorescent probes. *Osteoarthritis Cartilage* 2004; 12: 239–244.
24. Gao X, Yang L, Petros JA, Marshall FF, Simons JW, Nie S. In vivo molecular and cellular imaging with quantum dots. *Curr Opin Biotechnol* 2005; 16: 63–72.
25. Michalet X, Pinaud FF, Bentolila LA *et al.* Quantum dots for live cells, in vivo imaging, and diagnostics. *Science* 2005; 307: 538–544.
26. Voura EB, Jaiswal JK, Mattoussi H, Simon SM. Tracking metastatic tumor cell extravasation with quantum dot nanocrystals and fluorescence emission-scanning microscopy. *Nat Med* 2004; 10: 993–998.
27. Howarth M, Takao K, Hayashi Y, Ting AY. Targeting quantum dots to surface proteins in living cells with biotin ligase. *Proc Natl Acad Sci U S A* 2005; 102: 7583–7588.
28. Stroh M, Zimmer JP, Duda DG *et al.* Quantum dots spectrally distinguish multiple species within the tumor milieu in vivo. *Nat Med* 2005; 11: 678–682.
29. Colton HM, Falls JG, Ni H *et al.* Visualization and quantitation of peroxisomes using fluorescent nanocrystals: treatment of rats and monkeys with fibrates and detection in the liver. *Toxicol Sci* 2004; 80: 183–192.
30. Gupta AK, Gupta M. Synthesis and surface engineering of iron oxide nanoparticles for biomedical applications. *Biomaterials* 2005; 26: 3995–4021.
31. Talelli M, Rijcken CJ, Lammers T *et al.* Superparamagnetic iron oxide nanoparticles encapsulated in biodegradable thermosensitive polymeric micelles: toward a targeted nanomedicine suitable for image-guided drug delivery. *Langmuir* 2009; 25: 2060–2067.
32. Cho W, Cho M, Kim SR *et al.* Pulmonary toxicity and kinetic study of Cy5.5-conjugated superparamagnetic iron oxide nanoparticles by optical imaging. *Toxicol Appl Pharmacol* 2009; 239: 106–115.
33. Mahmoudi M, Simchi A, Milani AS, Stroeve P. Cell toxicity of superparamagnetic iron oxide nanoparticles. *J Colloid Interface Sci* 2009; 336: 510–518.
34. Paul KG , Frigo TB, Groman JY, Groman EV. Synthesis of ultrasmall superparamagnetic iron oxides using reduced polysaccharides. *Bioconjug Chem* 2004; 15: 194–401.
35. Chen TJ, Cheng TH, Chen CY. Targeted Herceptin-dextran iron oxide nanoparticles for noninvasive imaging of HER2/neu receptors using MRI. *J Biol Inorg Chem* 2009; 14: 253–260.
36. Weissleder R , Elizondo G, Wittenberg J, Lee AS, Josephson L, Brady TJ. Ultrasmall superparamagnetic iron oxide: an intravenous contrast agent for assessing lymph nodes with MR imaging. *Radiology* 1990; 175: 494–498.
37. Smith PK, Krohn RI, Hermanson GT *et al.* Measurement of protein using bicinchoninic acid. *Anal Biochem* 1985; 150: 76–85.
38. Angra P, Ridderhof J, Smithwick R. Comparison of two different strengths of carbol fuchsin in Ziehl–Neelsen staining for detecting acid-fast bacilli. *J Clin Microbiol* 2003; 41: 3459.
39. Woods A, Ellis R. *Pigments, minerals, and other tissue deposits in Laboratory Histopathology- A Complete Reference*, 1st edn. New York, NY: Churchill Livingstone, 1994; 8–11.
40. Wang J, Wakeham J, Harkness R, Xing Z. Macrophages are a significant source of type 1 cytokines during mycobacterial infection. *J Clin Invest* 1999; 103: 1023–1029.
41. Lee H, Yoon T, Weissleder R. Ultrasensitive detection of bacteria using core-shell nanoparticles and an NMR-filter system. *Angew Chem Int Ed* 2009; 48: 5657–5660.
42. Nishie A, Yoshimitsu K, Nakayama T *et al.* In vitro imaging of human monocytic cellular activity using superparamagnetic iron oxide. *Comput Med Imaging Graph* 2007; 31: 638–642.
43. von Zur Muhlen C, von Elverfeldt D, Bassler N *et al.* Superparamagnetic iron oxide binding and uptake as imaged by magnetic resonance is mediated by the integrin receptor Mac-1 (CD11b/CD18): implications on imaging of atherosclerotic plaques. *Atherosclerosis* 2007; 193: 102–111.